10486 *Biochemistry* **2009,** *48,* 10486–10491
DOI: 10.1021/bi901436m

BIOCHEMISTRY
including biophysical chemistry & molecular biology
Accelerated Publication

Picosecond Fluorescence Relaxation Spectroscopy of the Calcium-Discharged Photoproteins Aequorin and Obelin[†]

Bart van Oort,[‡] Elena V. Eremeeva,[§,⊥] Rob B. M. Koehorst,[‡,∥] Sergey P. Laptenok,[‡,§] Herbert van Amerongen,[‡,∥] Willem J. H. van Berkel,[§] Natalia P. Malikova,[⊥] Svetlana V. Markova,[⊥] Eugene S. Vysotski,[⊥] Antonie J. W. G. Visser,[§,∥] and John Lee*[,⊗]

[‡]*Laboratory of Biophysics and* [§]*Laboratory of Biochemistry and* [∥]*Microspectroscopy Centre, Wageningen University, 6703HA Wageningen, The Netherlands,* [⊥]*Photobiology Laboratory, Institute of Biophysics, Russian Academy of Sciences, Siberian Branch, 660036 Krasnoyarsk, Russia, and* [⊗]*Department of Biochemistry and Molecular Biology, University of Georgia, Athens, Georgia 30602*

Received August 16, 2009; Revised Manuscript Received September 21, 2009

ABSTRACT: Addition of calcium ions to the Ca^{2+}-regulated photoproteins, such as aequorin and obelin, produces a blue bioluminescence originating from a fluorescence transition of the protein-bound product, coelenteramide. The kinetics of several transient fluorescent species of the bound coelenteramide is resolved after picosecond-laser excitation and streak camera detection. The initially formed spectral distributions at picosecond-times are broad, evidently comprised of two contributions, one at higher energy ($\sim$25 000 cm^{-1}) assigned as from the Ca^{2+}-discharged photoprotein-bound coelenteramide in its neutral state. This component decays much more rapidly ($t_{1/2} \sim 2$ ps) in the case of the Ca^{2+}-discharged obelin than aequorin ($t_{1/2} \sim 30$ ps). The second component at lower energy shows several intermediates in the 150−500 ps times, with a final species having spectral maxima 19 400 cm^{-1}, bound to Ca^{2+}-discharged obelin, and 21 300 cm^{-1}, bound to Ca^{2+}-discharged aequorin, and both have a fluorescence decay lifetime of 4 ns. It is proposed that the rapid kinetics of these fluorescence transients on the picosecond time scale, correspond to times for relaxation of the protein structural environment of the binding cavity.

Bioluminescent animals are found in a variety of types occurring both terrestrially and in the ocean. More often than not, the chemistry of their light emission processes and the proteins involved are found quite unrelated. Well-studied cases, for example, are the bioluminescence of the firefly, which involves ATP and a substrate firefly luciferin, a benzthiozole derivative, and that of the photoprotein aequorin from the bioluminescent jellyfish *Aequorea*, which is triggered for light emission by Ca^{2+}. Coelenterazine, an imidazopyrazinone derivative (Figure 1), is the luciferin (a generic term for the substrate) involved in many marine bioluminescent systems, including the ones subject to this present study, the Ca^{2+}-regulated photoproteins, aequorin and obelin from the hydrazoan *Obelia* (*1*−*3*).

A significant advance in uncovering the mechanism of bioluminescence from aequorin and obelin resulted from the determination of the high-resolution spatial structure of the two photoproteins (*4*−*6*). The coelenterazine was revealed residing in an internal cavity substituted with a peroxy group (Figure 1B), as long suspected from earlier indirect evidence (*7*). Such a compound would be very unstable in free solution, but in the protein it appears to be frozen in place via a H-bond network to amino acid residues comprising the binding cavity. Model chemiluminescence studies with coelenterazine analogues had shown such a peroxide to be an intermediate, closing to a dioxetanone in the reaction pathway (*8*). The free energy produced by decarboxylation of this dioxetanone around 70 kcal/mol is sufficient to account for the energy of the photons of blue bioluminescence.

Aequorin and obelin are EF-hand proteins belonging to the large family of Ca^{2+}-binding proteins. They each contain three Ca^{2+}-ligating loops, and the spatial structure revealed how Ca^{2+} binding could lead to residue shifts in the binding site to interfere with the H-bond network and cause the decarboxylation reaction to proceed to the product coelenteramide (Figure 1C) in its first singlet electronic excited state (*2*). The bioluminescence spectrum then originates from the fluorescence transition of coelenteramide.

The bioluminescence spectra are broad with maxima depending on the type of organism. Aequorin has a maximum at 469 nm and various obelins at 475−495 nm (*9*). The photoproteins are hardly fluorescent themselves, but following the bioluminescence reaction, the Ca^{2+}-discharged photoproteins exhibit strong fluorescence. For Ca^{2+}-discharged aequorin, the fluorescence spectral distribution is very similar to the bioluminescence spectrum. In contrast, the Ca^{2+}-discharged obelins show fluorescence maxima about 25 nm to longer wavelength than their bioluminescence. Furthermore, the obelin bioluminescence spectrum is bimodal, with a minor higher energy band having a maximum around 400 nm, not evident in aequorin bioluminescence (*9*, *10*). From spectral studies of model compounds, this high energy band is identified as from the excited level of

[†]This work was supported by NATO Collaborative Linkage Grant No. 979229, Grants of SB RAS and RFBR 09-04-12022, MCB program of RAS. B.v.O. was supported by "Stichting voor Fundamenteel Onderzoek der Materie (FOM)", which is financially supported by the NWO, and by a Rubicon grant of NWO. E.V.E. was supported by Wageningen University Sandwich Ph.D.-Fellowship program. S.P.L was supported by Wageningen University Sandwich Ph.D.-Fellowship program, European Community (Marie Curie Research Training Network MRTN-CT-2005-019481 (From FLIM to FLIN), and Computational Science Grant 635.000.014 from the Netherlands Organization for Scientific Research.

*To whom correspondence should be addressed. E-mail jlee@uga.edu; phone +1-706-549-4630; fax +1-706-542-1738.

 Published on Web 10/07/2009

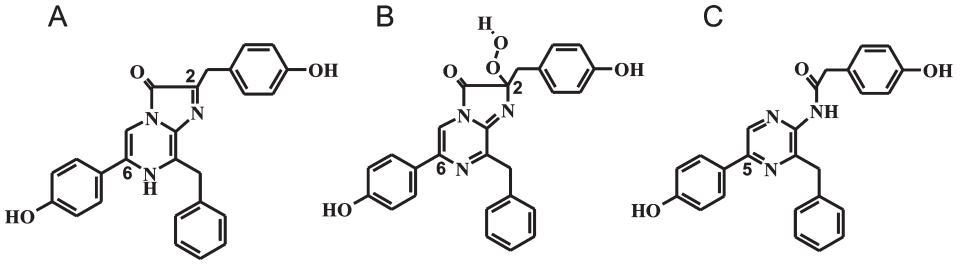

FIGURE 1: Chemical structures of coelenterazine (A), 2-hydroperoxycoelenterazine (B), and coelenteramide (C).

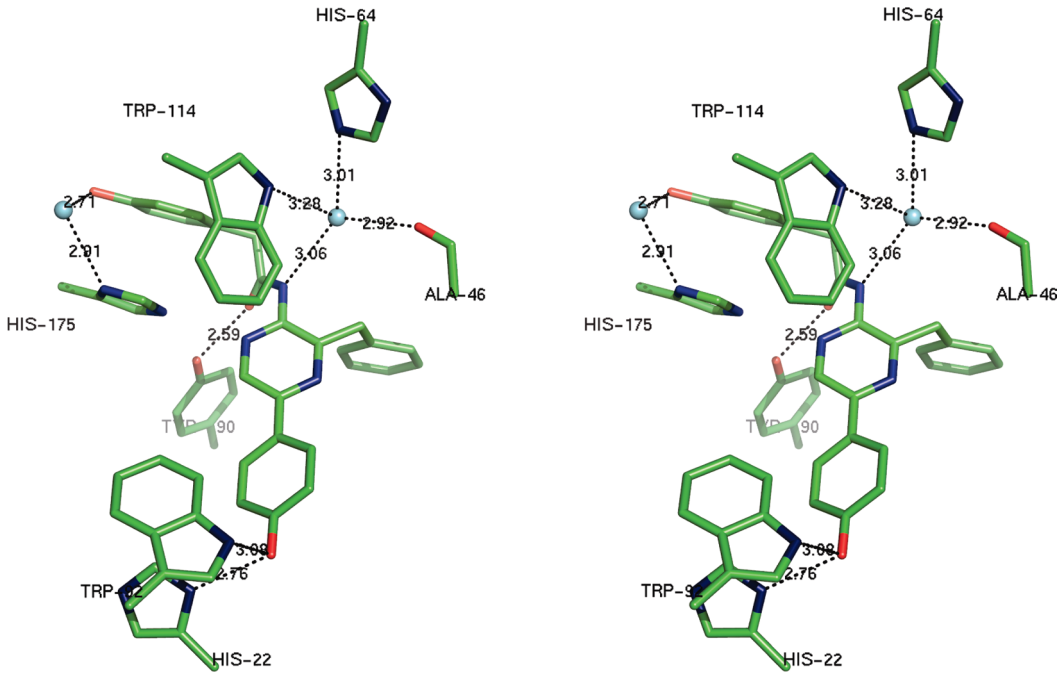

FIGURE 2: Stereoview showing the interactions of coelenteramide within the binding cavity of Ca^{2+}-discharged obelin (PDB code 2F8P). The blue balls represent water molecules; dotted lines indicate H-bonds. The distances are shown in Ångstroms. Hydrogen bonds (dotted lines) were determined with the PyMOL program (*33*).

coelenteramide in its neutral state (*11*). More controversial has been the characterization of the lower energy blue bioluminescence band because the evidence from fluorescence model diagnostics is somewhat ambiguous. The spatial structures of obelin and its product, however, directly implicate the origin of the blue band as from the excited coelenteramide 5-phenoxy anion. The primary excited neutral coelenteramide should be quickly transformed to the anion due to the proximity of a His22 residue, H-bonded to the phenolic oxygen and poised to act as a proton acceptor (Figure 2) (*2*). By such a mechanism, the bioluminescence spectrum is "tuned" to most efficiently satisfy the biological survival function of the light emission.

It is the purpose of this work to investigate the excited state dynamics of coelenteramide bound in the protein cavity, to test this proton transfer idea, and also to account for the variations in steady-state emission properties.

EXPERIMENTAL PROCEDURES

Preparation of Proteins. The apoobelin and apoaequorin truncated by residues from the N-terminus were produced in transformed *E. coli* BL21-Gold (*12*, *13*) and purified and charged with coelenterazine to form the active photoproteins, all as previously reported (*14*, *15*). The final products were homogeneous according to SDS-PAGE. To prepare the Ca^{2+}-discharged samples, the concentrated solutions of photoproteins were diluted to a concentration of 0.26 mg/mL (aequorin) and 0.32 mg/mL (obelin) with 50 mM Bis-Tris propane pH 7.0 containing $CaCl_2$ (final concentration of calcium in a sample = 1 mM). Fluorescence was measured after the bioluminescence reaction ceased (OD was 0.06−0.07 at the excitation wavelengths) and samples were deoxygenated by flushing with argon then applying vacuum.

Time-Resolved Fluorescence. Time resolved fluorescence was measured at room temperature with a streak camera setup as described in detail in ref *16*. In brief, the sample is excited by ~0.2 ps duration pulses (340 nm, ~1 mW) at a repetition rate of 250 kHz. Pulses were generated in an optical parametric amplifier that was fed by pulses from a mode-locked titanium-sapphire laser, amplified by a regenerative amplifier. Polarization was set vertical by a Berek polarizer. The samples were in a static fluorescence cuvette (10 mm × 10 mm). Fluorescence was collected under magic angle polarization and focused by a set of achromatic lens assemblies onto the slit of the imaging spectrograph. The spectrograph focused the output light (horizontal spectral dispersion) directly onto the stripe-shaped cathode of the streak camera. The resulting photoelectrons are accelerated and deflected by a time-dependent vertical electric field and detected by a multichannel plate, phosphorescent screen, and a CCD camera. Scale, linearity, and curving of the time and wavelength axes were extensively treated as described in

ref *16*. For more details on streak camera experiments and data analysis, see ref *17*.

The CCD images are two-dimensional data sets of fluorescence intensity as a function of time and wavelength. For the experiments described here, the time windows were 160 ps or 2 ns, and the spectral window ranged from 330 to 650 nm (using a grating with 40 grooves/mm ruling and 500 nm blaze). The images contain the initial part of the decay (directly after excitation), overlapped with the decay at a delay of 6.6 ns (backsweep). The backsweep is treated explicitly in data analysis and gives information on slower relaxation processes. In addition to fluorescence, the CCD images also show Rayleigh and Raman scatter. Wavelengths at which the scatter intensity was high relative to the fluorescence were omitted from analysis. When the scatter intensity was of the same order as fluorescence intensity, the scatter was included explicitly in the fitting as a component with an infinitely fast decay as described in ref *17*.

Data Analysis. Streak data were analyzed in two distinct ways. First, the data were fitted to a sequential model, in which a spectral species i evolves into species $i + 1$ with rate k_i, and then into $i + 2$ with rate k_{i+2}, and so on. The fitting procedure is described in detail in ref *18*. In this procedure, spectral shapes are unconstrained. To increase the signal-to-noise ratio, the decays were averaged over 5 nm prior to fitting (this corresponds to 313 cm^{-1} at 400 nm and 139 cm^{-1} at 600 nm).

Second, the data were converted to an energy scale (dividing the fluorescence intensity at each detection wavelength by the square of the detection wavelength). The data were then fitted to a sum of two spectral bands: one with a Gaussian shape and one with a log-normal shape. Position and intensity of the two bands were fitted to exponential functions. The fitting procedure and software are described in detail elsewhere (*19*). The data could also be fitted with a sum of three or four Gaussian shapes, however, that required more fit parameters and led to strong correlations (and large uncertainties) between the fitted values. Fitting with two log-normal functions yields one distribution with skewness close to unity, and this function was therefore replaced by a Gaussian. Gaussian and log-normal lineshapes very adequately describe fluorescence emission spectra for a range of (bio)organic chromophores (*20*). As a consequence, this fitting procedure has the advantage over the first fitting procedure that it is closer to a physically meaningful description of the data. Unfortunately it has a reduced time resolution (~25 ps).

The estimated errors of the peak positions were calculated as standard errors from the fits of the spectra. The uncertainty of the lifetimes cannot be judged from the standard errors due to strong correlations between the fit parameters. Instead the uncertainty of a lifetime is deduced from the fit quality of the best fit obtained when that lifetime is fixed at a range of different values.

RESULTS

Figure 3 shows that the fluorescence decay function of the Ca^{2+}-discharged aequorin is multiexponential and depends on the wavelength of detection. This indicates that the excitation of protein-bound coelenteramide populates at least two excited states, with a rapidly decaying high-energy state. The data can also be presented as spectra at different times after excitation. Figure 4 (top) shows such time-resolved emission spectra (TRES)[1] of Ca^{2+}-discharged aequorin at various times following the excitation, and indeed, a fast decaying spectral band does appear at the higher energy side. On the assumption of a log-normal and a Gaussian energy distribution (see above for reasons to use these bandshapes), the TRES are resolved into the two

[1]Abbreviations: TRES, time resolved emission spectra.

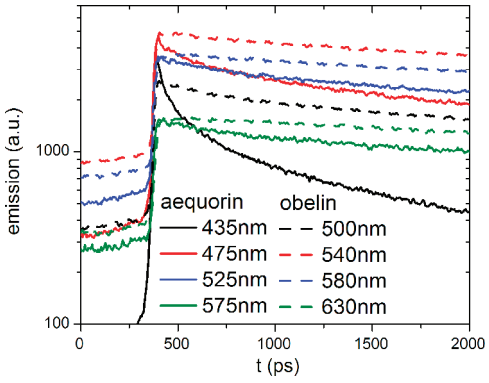

FIGURE 3: Fluorescence decay curves of Ca^{2+}-discharged aequorin and obelin (dashed) at several detection wavelengths. The decays are averaged over 3 nm around the indicated central wavelengths. The signal before about 300 ps is due to the backsweep (see Experimental Procedures).

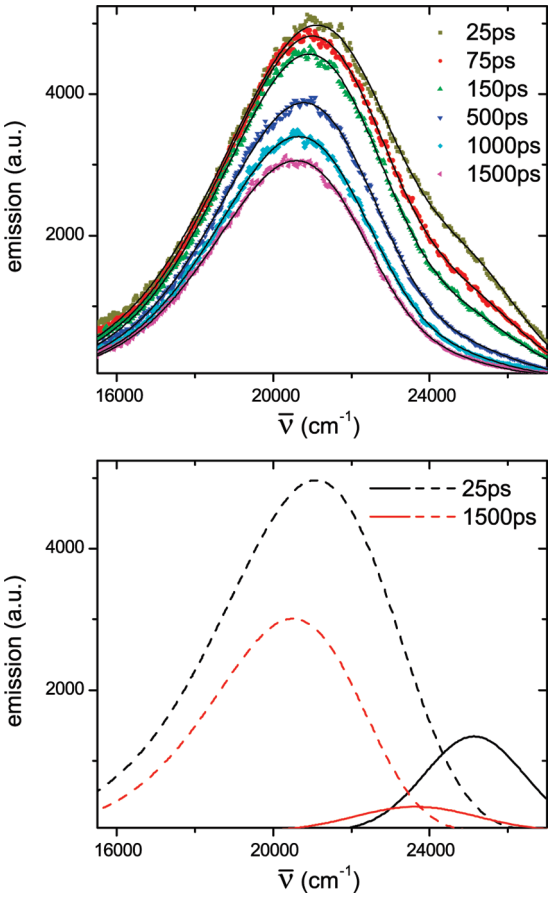

FIGURE 4: Time-resolved emission spectra of Ca^{2+}-discharged aequorin at various times after excitation. The spectrum at each time is fitted as a sum of a log-normal (dashed) and Gaussian function. The lower panel shows the two functions at 25 ps and 1.5 ns after excitation. At 25 ps, the log-normal function peaks at 21 100 cm^{-1} (465 nm) and the Gaussian function at 25 900 cm^{-1} (396 nm). At 1.5 ns this is 20 500 cm^{-1} (480 nm) and 23 600 cm^{-1} (419 nm). The peak positions in nanometers were obtained from converting the fitted functions to a wavelength scale using $F(\lambda) = (dN/d\lambda) = \bar{\nu}^2(dN/d\bar{\nu}) = \bar{\nu}^2F(\bar{\nu})$, with λ in m and $\bar{\nu}$ in m^{-1} (*23*).

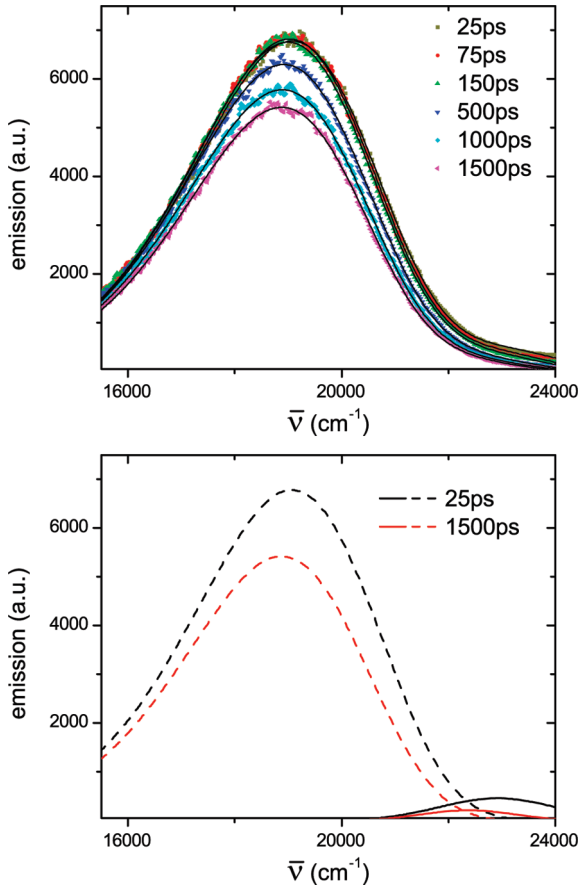

FIGURE 5: Time-resolved emission spectra of Ca^{2+}-discharged obelin at various times after excitation. The spectrum at each time is fitted as a sum of a log-normal and Gaussian function. The lower panel shows the two functions at 25 ps and 1.5 ns after excitation. At 25 ps, the log-normal function peaks at 19 000 cm^{-1} (517 nm) and the Gaussian function at 22 900 cm^{-1} (435 nm). At 1.5 ns, this is 18 900 cm^{-1} (522 nm) and 22 400 cm^{-1} (446 nm). The peak positions in nanometers were obtained from converting the fit functions to a wavelength scale, see legend of Figure 4.

bands, shown for 25 and 1500 ps after excitation in Figure 4 (bottom). TRES at each detection time were fitted with two bands. The higher energy band (25 900(30) cm^{-1} at 25 ps) decays with a 1/e lifetime of approximately 45(15) ps, while redshifting ~2200(100) cm^{-1} with a 1/e lifetime of 630(50) ps. The values in parentheses are standard errors calculated from the fit of the spectra (for the peak positions) and uncertainties calculated as described in the Experimental Procedures (for the lifetimes). In addition to the 45 ps decay component, there is a small component with ~4 ns decay. The low energy band (21 000(20) cm^{-1} at 25 ps) shifts 670(50) cm^{-1} in 260(50) ps and shows a slower redshift of 380(30) cm^{-1} in ~4 ns. The intensity of this 21 000 cm^{-1} band decays biexponentially: 40% with a lifetime of 500(50) ps and 60% 2.7 ns.

Ca^{2+}-discharged obelin exhibits less spectral change with time than Ca^{2+}-discharged aequorin. Figure 5 shows the TRES for Ca^{2+}-discharged obelin at various times after excitation. The main (low energy) band (19 070(50) cm^{-1} at 25 ps) shifts ~230(30) cm^{-1}, with a 1/e lifetime of approximately 190 ps, with a slower (~4 ns) further shift of 100(10) cm^{-1}. In addition, there is a small high energy band (22 770(50) cm^{-1} at 25 ps) that shifts ~490(50) cm^{-1} in 200 ps. This band lies between the two bands of Ca^{2+}-discharged aequorin. A band with higher energy (> 24 000 cm^{-1}) may be present but must then be very shortlived.

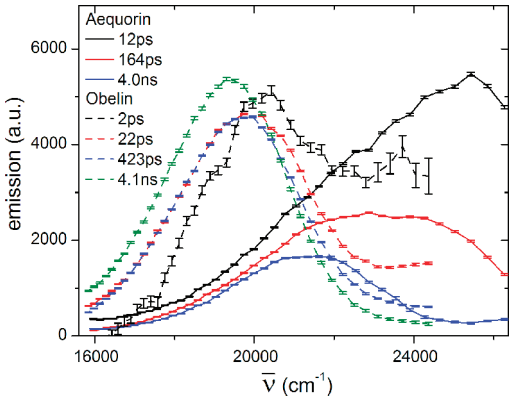

FIGURE 6: Fit results of streak data with a 180 ps time basis for evolution associated fluorescence decay spectra $I(\bar{\nu})$ of Ca^{2+}-discharged aequorin and obelin. The initial spectrum of Ca^{2+}-discharged obelin (black dashed line) is bimodal with significant intensity of the higher energy band in the same region as the initial spectrum of Ca^{2+}-discharged aequorin (black full line). The lower energy band of obelin after spectral deconvolution analysis (Figure 4) overlaps with the 12 ps band from Ca^{2+}-discharged aequorin spectrum. It can be concluded that if a high-energy form of Ca^{2+}-discharged obelin is present shortly after excitation, it does not exist for longer than ~1 ps. The bars indicate standard errors.

This is verified by an experiment using < 3 ps resolution in Figure 6. This figure shows the results of fitting the fluorescence decay data with a four-component sequential model. The evolution of the initial Ca^{2+}-discharged obelin spectrum (dashed black curve in Figure 6) to the second spectrum occurs on a time scale that is on the limit of the time resolution of the setup. As a consequence, both the time and spectrum of this initial component are not determined very accurately. It is however clear that the Ca^{2+}-discharged obelin spectrum shows significant intensity up to at least 24 400 cm^{-1} (~300 cm^{-1} resolution). The second spectrum, peaking at 20 000 cm^{-1}, evolves into a spectrum peaking at 19 660 cm^{-1} in 22(1) ps and then into the final emitting state at 19 400 cm^{-1} in 423(17) ps. The values in parentheses are standard errors obtained from the fit. The fluorescence lifetime of the final emitting species is ~4 ns. The streak camera setup is not very sensitive for the amplitude and lifetime of fluorescence decays longer that 1 ns (for details see ref *17*). This is probably why the amplitude of the final emitting species is higher than that of the third species. The presence of a ~4 ns fluorescence decay time is confirmed by time-correlated single-photon counting experiments using the setup described in refs (*21* and *22*) (data not shown).

The spectral evolution of Ca^{2+}-discharged aequorin on this fast time scale is very different. The initial fluorescence emission spectrum of aequorin red-shifts from 25 400 to 23 000 cm^{-1} in 12.0(0.1) ps (black curve in Figure 6) and then further to the final emitting state at 21 300 cm^{-1} in 164(3) ps. The fluorescence lifetime of the final emitting state is ~4 ns, again confirmed by time-correlated single-photon counting experiments.

Most published spectra are in units of photons/wavelength interval versus wavelength. For comparison, the wavenumber maxima $\bar{\nu}_M$ in the present results can be converted to the equivalent wavelength maximum, λ_M, by the expression (*23*):

$$\lambda_M = \bar{\nu}_M{}^{-1}\left[1 - 0.36\left(\frac{\text{fwhm}}{\bar{\nu}_M}\right)^2\right]$$

in which fwhm is the full width at half-maximum of the spectral (Gaussian) band. Although this equation is formally not correct

for log-normal distributions, in practice it provides accurate results. For our fits, it gives deviations of less than 1 nm when compared with the maxima derived from conversion of the log-normal distribution from an energy to a wavelength scale using $F(\lambda) = (dN/d\lambda) = \bar{\nu}^2(dN/d\bar{\nu}) = \bar{\nu}^2F(\bar{\nu})$, with λ in m and $\bar{\nu}$ in m^{-1} (*23*).

DISCUSSION

In this work, we have investigated the excited state dynamics of coelenteramide bound in the protein cavities of the calcium-discharged photoproteins aequorin and obelin. Excitation at 340 nm into the lowest energy absorption band generates the neutral coelenteramide in its lowest electronically excited (S_1) state. In aqueous solution, the fluorescence of free coelenteramide is quenched, but in less polar solvents, the inhomogeneously broadened spectrum has a maximum spanning the range 386−423 nm, depending on solvent polarity. Free coelenteramide in solutions that are made basic, however, displays a new fluorescence band at lower energy, spectral maxima 465−520 nm, again depending on solvent polarity and also somewhat on basicity. This lower energy band is identified as the 5-phenoxy anion based on the fact that in the excited state, the p*K** of phenols is known to be 5 or more units more acidic than the ground state p*K* around 10, and this is where dissociation is likely to occur as the other phenol, the 2-hydroxybenzyl substituent, is not conjugated to the main ring system. The amide is not considered acidic although, using analogues with the phenoxy blocked say by methylation or absent altogether, the amide proton can be dissociated with a very strong base such as tertiary butoxide in dimethyl sulfoxide (DMSO) to produce what is apparently the coelenteramide amide anion, having fluorescence band maxima in the range 420−450 nm.

Therefore, the two excited states suggested as being formed in the binding site cavities of the Ca^{2+}-discharged photoproteins (Figures 3−6) are first the neutral coelenteramide, which reverts to the anion on a picosecond time scale. Unfortunately, any corresponding rise in the longer wavelength band is not recoverable in the analysis suggesting an ultrafast kinetic process. In the binding site cavity of Ca^{2+}-discharged obelin (Figure 2), it is observed that His22 is in a strong H-bond interaction with the 5-phenolic oxygen, inferred by the N−O separation of 2.76 Å (*24*). An elementary picture of such an H-bond is one in which partial positive charge is deposited from the donor oxygen onto the acceptor nitrogen, in other words, some partial dissociation of the phenol even in the ground state so that in the excited state having the lowered p*K**, a more complete transfer of charge takes place. This idea is supported by a computational study (*25*), and it has been suggested from properties of fluorescence models (*26*) that a complete ion-pair is formed. In any case, the time-scale for such a proton shift within the already formed H-bond must be subpicosecond. The decay of the neutral band intensity as the excited anion band increases over a time about 45 ps (Figure 4) is more likely a measure of the structural relaxation of the binding cavity, the origin of the inhomogeneous broadening of the protein-bound fluorescence (*27*).

It has already been proposed that the bioluminescence reaction generates these same two excited states (*24*). The structural evidence suggests that the primary excited species populated by the free energy released by the decarboxylation of the peroxy-coelenterazine in obelin is the neutral coelenteramide which, as already described, rapidly dissociates to the excited anion by means of the proximity of His22 to the 5-phenol group.

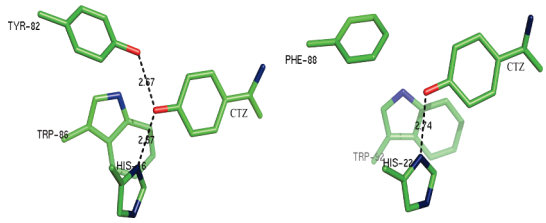

FIGURE 7: Interactions between the hydroxyl moiety of the 6-hydroxyphenyl substituent of coelenterazine within the binding cavity of aequorin (left) and obelin (right). Hydrogen bonds (dotted lines) were determined with the PyMOL program (*33*). The distances are shown in Ångstroms.

This His22 is found in the same position in the structure of the cavity in both obelin and Ca^{2+}-discharged obelin, and also an equivalent His16 is in the same position in the aequorin cavity. Further evidence for the presence of two excited species comes from the bioluminescence of obelin, which reveals a small contribution at the high energy end not seen in aequorin bioluminescence. It was suggested that the total bioluminescence spectrum results from a competition between the radiation rate from the primary neutral excited state and the rate of population of the excited anion.

Qualitative support for the idea that H-bonding to the oxygen at the 6-phenol position controls the emission spectra has been obtained from study of a number of aequorin and obelin mutants (*10*, *28*−*31*). The substitution of Trp92 in obelin (*29*, *30*) and Trp86 (*28*) in aequorin, which are found not far away from the oxygen atom of the 6-(*p*-hydroxyphenyl) group of coelenterazine (Figure 7, right) to phenylalanine, led to the appearance of bimodal bioluminescence with a prominent contribution from the 400 nm neutral species of coelenteramide. The substitution Trp92Arg in obelin gives an almost monomodal emission around 400 nm, with almost no contribution from the excited anion (*31*).

Figure 7 (left) shows that aequorin has two H-bonds to the 6-phenol oxygen of coelenterazine. Replacing aequorin's Tyr82 by phenylalanine, thus removing that hydrogen bond, shifts its emissions to lower energy, mimicking obelin, with a bioluminescence maximum at 500 nm and fluorescence at 495 nm. Likewise, changing obelin's Phe88 to tyrosine, adding the hydrogen bond as in aequorin, upshifts the energy levels near those from aequorin, the bioluminescence maximum now being at 453 nm and the fluorescence maximum at 487 nm.

It needs to be appreciated that the properties of the excited states and their corresponding emissions will depend to some extent on the process of excitation. Fluorescence excitation (photon absorption) is a Franck−Condon transition; therefore, the initial hot state is on the energy envelope of the cavity interactions which have to cool to the lowest level of the excited state. The bioluminescence energetic process goes by an adiabatic crossing of the reaction coordinate with the cavity relaxation energy envelope of the bound product coelenteramide, a crossing so as to direct the reaction energy to efficiently populate the excited state of the product (*32*). Evidently, from the 25 nm shift of the fluorescence maximum over the bioluminescence, the final equilibrated state of Ca^{2+}-discharged obelin must lie at somewhat lower energy than the bioluminescence emitting state.

Rationalization of these perturbation effects needs to be done with caution in the absence of spatial structures for each of these mutants. Especially conjectural is any explanation of how the H-bonds control the probability of excited anion emission. It can be expected that a combination of the structural and fluorescence

dynamics measurements, perhaps combined with theoretical computation (*25*), could lead to a quantitative account of how protein cavity structure quantitatively modulates the spectral properties.

REFERENCES

1. Shimomura, O. (2006) Bioluminescence: Chemical Principles and Methods , World Scientific Publishing, Singapore.
2. Vysotski, E. S., and Lee, J. (2004) Ca^{2+}-regulated photoproteins: structural insight into the bioluminescence mechanism. *Acc. Chem. Res. 37*, 405–415.
3. Vysotski, E. S., Lee, J. (2007) Bioluminescent mechanism of Ca^{2+}-regulated photoproteins from three-dimensional structures. In Luciferases and Fluorescent Proteins: Principles and Advances in Biotechnology and Bioimaging (Viviani, V. R., Ohmiya, Y., Eds.), pp. 19−41, Transworld Research Network, Kerala, India.
4. Head, J. F., Inouye, S., Teranishi, K., and Shimomura, O. (2000) The crystal structure of the photoprotein aequorin at 2.3 Å resolution. *Nature 405*, 372–376.
5. Liu, Z.-J., Vysotski, E. S., Chen, C.-J., Rose, J., Lee, J., and Wang, B.-C. (2000) Structure of the Ca^{2+}-regulated photoprotein obelin at 1.7 Å resolution determined directly from its sulfur substructure. *Protein Sci. 9*, 2085–2093.
6. Liu, Z.-J., Vysotski, E. S., Deng, L., Lee, J., Rose, J., and Wang, B.-C. (2003) Atomic resolution structure of obelin: soaking with calcium enhances electron density of the second oxygen atom substituted at the C2-position of coelenterazine. *Biochem. Biophys. Res. Commun. 311*, 433–439.
7. Shimomura, O., and Johnson, F. H. (1978) Peroxidized coelenterazine, the active group in the photoprotein aequorin. *Proc. Natl. Acad. Sci. U.S.A. 75*, 2611–2615.
8. McCapra, F., and Chang, Y. C. (1967) The chemiluminescence of a *Cypridina* luciferin analogue. *Chem. Commun.* 1011–1012.
9. Markova, S. V., Vysotski, E. S., Blinks, J. R., Burakova, L. P., Wang, B.-C., and Lee, J. (2002) Obelin from the bioluminescent marine hydroid *Obelia geniculata*: cloning, expression, and comparison of some properties with those of other Ca^{2+}-regulated photoproteins. *Biochemistry 41*, 2227–2236.
10. Stepanyuk, G. A., Golz, S., Markova, S. V., Frank, L. A., Lee, J., and Vysotski, E. S. (2005) Interchange of aequorin and obelin bioluminescence color is determined by substitution of one active site residue of each photoprotein. *FEBS Lett. 579*, 1008–1014.
11. Shimomura, O., and Teranishi, K. (2000) Light-emitters involved in the luminescence of coelenterazine. *Luminescence 15*, 51–58.
12. Markova, S. V., Vysotski, E. S., Lee, J. (2001) Obelin hyperexpression in *E. coli*, purification and characterization. In Bioluminescence and Chemiluminescence (Case, J. F., Herring, P. J., Robison, B. H., Haddock, S. H. D., Kricka, L. J., Stanley, P. E., Eds.), pp 115−119, World Scientific Publishing Co., Singapore.
13. Deng, L., Vysotski, E. S., Markova, S. V., Liu, Z.-J., Lee, J., Rose, J., and Wang, B.-C. (2005) All three Ca^{2+}-binding loops of photoproteins bind calcium ions: the crystal structures of calcium-loaded apoaequorin and apo-obelin. *Protein Sci. 14*, 663–675.
14. Illarionov, B. A., Frank, L. A., Illarionova, V. A., Bondar, V. S., Vysotski, E. S., and Blinks, J. R. (2000) Recombinant obelin: cloning and expression of cDNA purification, and characterization as a calcium indicator. *Methods Enzymol. 305*, 223–249.
15. Vysotski, E. S., Liu, Z.-J., Rose, J., Wang, B.-C., and Lee, J. (2001) Preparation and X-ray crystallographic analysis of recombinant obelin crystals diffracting to beyond 1.1 Å. *Acta Crystallogr. Sect. D: Biol. Crystallogr. 57*, 1919–1921.
16. Van Oort, B., Murali, S., Wientjes, E., Koehorst, R. B. M., Spruijt, R., van Hoek, A., Croce, R., and van Amerongen, H. (2009) Ultrafast resonance energy transfer from a site-specifically attached fluorescent chromophore reveals the folding of the N-terminal domain of CP29. *Chem. Phys. 357*, 113–119.
17. Van Stokkum, I. H. M., van Oort, B., van Mourik, F., Gobets, B., van Amerongen, H. (2008) (Sub-)Picosecond spectral evolution of fluorescence studied with a synchroscan streak-camera system and target analysis. In Biophysical Techniques in Photosynthesis (Aartsma, T. J., Matysik, J., Eds.), Vol. II, pp 223−240, Springer, Dordrecht, The Netherlands.
18. Mullen, K. M., and van Stokkum, I. H. M. (2007) TIMP: an R package for modeling multi-way spectroscopic measurements. *J. Stat. Soft. 18*, 2007.
19. Koehorst, R. B. M., Laptenok, S., van Oort, B., van Hoek, A., Spruijt, R. B., van Stokkum, I. H. M., van Amerongen, H., and Hemminga, M. A. (2009) Profiling of dynamics in protein-lipid-water systems: A time-resolved fluorescence study of a model membrane protein with the label BADAN at specific membrane depths. Eur. Biophys. J. DOI: 10.1007/s00249-009-0538-6. Published Online: September 16, 2009.
20. Burstein, E. A., and Emelyanenko, V. I. (1996) Log-normal description of fluorescence spectra of organic fluorophores. *Photochem. Photobiol. 64*, 316–320.
21. Van Oort, B., van Hoek, A., Ruban, A. V., and van Amerongen, H. (2007) Equilibrium between quenched and nonquenched conformations of the major plant light-harvesting complex studied with high-pressure time-resolved fluorescence. *J. Phys. Chem. B 111*, 7631–7637.
22. Borst, J. W., Hink, M. A., van Hoek, A., and Visser, A. J. W. G. (2005) Effects of refractive index and viscosity on fluorescence and anisotropy decays of enhanced cyan and yellow fluorescent proteins. *J. Fluorescence 15*, 153–160.
23. Seliger, H. H. (1978) Excited states and absolute calibrations in bioluminescence. *Methods Enzymol. 57*, 560–600.
24. Liu, Z.-J., Stepanyuk, G. A., Vysotski, E. S., Lee, J., Markova, S. V., Malikova, N. P., and Wang, B.-C. (2006) Crystal structure of obelin after Ca^{2+}-triggered bioluminescence suggests neutral coelenteramide as the primary excited state. *Proc. Natl. Acad. Sci. U.S.A. 103*, 2570–2575.
25. Tomilin, F. N., Antipina, L. Yu., Vysotski, E. S., Ovchinnikov, S. G., and Gitelzon, I. I. (2008) Fluorescence of calcium-discharged obelin: The structure and molecular mechanism of emitter formation. *Biochem. Biophys. Mol. Biol. 422*, 279–284.
26. Mori, K., Maki, S., Niwa, H., Ikeda, H., and Hirano, T. (2006) Real light emitter in the bioluminescence of the calcium-activated photoproteins aequorin and obelin: light emission from the singlet-excited state of coelenteramide phenolate anion in a contact ion pair. *Tetrahedron 62*, 6272–6288.
27. Petushkov, V. N., van Stokkum, I. H. M., Gobets, B., van Mourik, F., Lee, J., van Grondelle, R., and Visser, A. J. W. G. (2003) Ultrafast fluorescence relaxation spectroscopy of 6,7-dimethyl-(8-ribityl)-lumazine and riboflavin, free and bound to antenna proteins from bioluminescent bacteria. *J. Phys. Chem. B 107*, 10934–10939.
28. Ohmiya, Y., Ohashi, M., and Tsuji, F. I. (1992) Two excited states in aequorin bioluminescence induced by tryptophan modification. *FEBS Lett. 301*, 197–201.
29. Vysotski, E. S., Liu, Z.-J., Markova, S. V., Blinks, J. R., Deng, L., Frank, L. A., Herko, M., Malikova, N. P., Rose, J. P., Wang, B.-C., and Lee, J. (2003) Violet bioluminescence and fast kinetics from W92F obelin: structure-based proposals for the bioluminescence triggering and the identification of the emitting species. *Biochemistry 42*, 6013–6024.
30. Deng, L., Vysotski, E. S., Liu, Z.-J., Markova, S. V., Malikova, N. P., Lee, J., Rose, J., and Wang, B.-C. (2001) Structural basis for the emission of violet bioluminescence from a W92F obelin mutant. *FEBS Lett. 506*, 281–285.
31. Malikova, N. P., Stepanyuk, G. A., Frank, L. A., Markova, S. V., Vysotski, E. S., and Lee, J. (2003) Spectral tuning of obelin bioluminescence by mutations of Trp92. *FEBS Lett. 554*, 184–188.
32. Chung, L. W., Hayashi, S., Lundberg, M., Nakatsu, T., Kato, H., and Morokuma, K. (2008) Mechanism of efficient firefly bioluminescence via adiabatic transition state and seam of sloped conical intersection. *J. Am. Chem. Soc. 130*, 12880–12881.
33. DeLano, W. L. (2002) The PyMOL Molecular Graphics System, DeLano Scientific, San Carlos, CA.